EEET ECOLOGICAL ENGINEERING & ENVIRONMENTAL TECHNOLOGY

Ecological Engineering & Environmental Technology, 2026, 27(6), 451–465
https://doi.org/10.12912/27197050/221847
ISSN 2719–7050, License CC-BY 4.0

Received: 2026.04.17
Accepted: 2026.05.18
Published: 2026.06.01

Aerodynamic performance of an Archimedes spiral wind turbine at low wind speed: A computational fluid dynamics study of blade angle variations

Sarwo Edhy Sofyan[1*], Muhammad Dhiaurrahman[1], Zulfadhli[1], Thaharul Fikri[1], Akram Tamlicha[1]

[1] Department of Mechanical Engineering, Universitas Syiah Kuala, Banda Aceh 23111, Indonesia
* Corresponding author's e-mail: sarwo.edhy@usk.ac.id

ABSTRACT

This study addresses the optimization of small-scale renewable energy systems for low-wind environments, aiming to improve wind energy utilization efficiency in regions with limited wind resources such as Indonesia. The aerodynamic performance of an Archimedes spiral wind turbine (ASWT) was numerically investigated using computational fluid dynamics (CFD) under varying blade inclination angles (30°, 35°, 40°, 45°, 50°, and 60°) at a constant wind speed of 5 m/s. The simulations were performed based on the Navier-Stokes framework using k-ε turbulence modelling with standard wall functions, enabling detailed analysis of flow behavior, torque generation, power output, and wake development. The results demonstrate that turbine performance strongly depends on blade inclination angle. Higher blade angles improved aerodynamic interaction, increasing torque and power output. The best performance was achieved at 60°, producing 29.691 W with 37% efficiency, while the 30° configuration showed the lowest performance at 21.076 W and 26% efficiency. Wake analysis indicated that larger blade angles enhanced momentum extraction and kinetic energy conversion, but also increased downstream flow disturbance. The simulation is performed under unsteady conditions, and the effects of atmospheric turbulence variation and structural deformation are not considered in this study. The findings provide practical value for the design of low-speed wind energy systems by identifying optimal geometric configurations for improved energy harvesting in low-wind regions. From an ecological engineering perspective, the results support the development of compact, efficient wind turbines capable of decentralized clean energy production, reducing reliance on fossil fuels in rural and urban low-wind environments. The originality of this work lies in the systematic CFD-based evaluation of blade inclination angle effects on Archimedes wind turbine performance under low wind speed conditions, supported by aerodynamic and wake-field analysis. The results contribute to a deeper understanding of spiral turbine behavior and provide a foundation for environmentally adaptive wind energy system design.

Keywords: renewable energy, computational fluid dynamics, wind turbine, aerodynamic performance.

INTRODUCTION

Global electricity demand continues to increase due to industrial growth, population expansion, and rising energy consumption, resulting in greater dependence on fossil fuels. This dependence has significantly contributed to greenhouse gas emissions, climate change, global warming, and environmental degradation (Budiman and Khoirunnisa, 2025). In response to these challenges, many countries are accelerating the transition toward sustainable and low-carbon energy systems through the development of renewable energy technologies (Ardoin and Bowers, 2025).

Indonesia has committed to reducing greenhouse gas emissions and increasing the share of renewable energy in its national energy mix (Pambudi et al., 2025). However, growing energy demand and declining fossil fuel reserves highlight the urgent need for sustainable and decentralized power generation systems, particularly in remote regions with limited infrastructure (Budiarto and

Surjosatyo, 2021). Therefore, small scale renewable energy technologies are considered essential for supporting environmental sustainability and low carbon development (Pandyaswargo et al., 2024).

Among various renewable energy sources, wind energy has emerged as a promising alternative because of its clean, sustainable, and environmentally friendly characteristics (Kusuma et al., 2024). Indonesia possesses considerable wind energy potential, with average wind speeds generally ranging from 3 to 7 m/s (Maulana et al., 2024). Although these wind speeds are relatively low compared with those in temperate regions, they remain suitable for specially designed low-wind-speed turbines. Consequently, the development of wind turbines capable of operating efficiently under low wind speed conditions is important for supporting decentralized sustainable energy systems in Indonesia.

One promising technology for low-wind-speed applications is the ASWT (Ortiz-Velázquez et al., 2026). Unlike conventional horizontal-axis wind turbines, which mainly rely on lift forces, the ASWT utilizes both lift and drag forces through its spiral blade configuration, enabling more effective energy extraction at low wind speeds (Kim et al., 2014). Due to these advantages, the ASWT has attracted increasing attention as a potential solution for small-scale renewable energy generation in areas with low wind potential.

Several studies have investigated the aerodynamic performance of the ASWT through computational and experimental approaches. Labib et al. (2020) examined blade angle effects on a small-scale ASWT using CFD, varying angles from 50° to 65° at wind speeds of 5 to 12 m/s, but the narrow angular range left the aerodynamic behavior below 50° unexplored. Kamal et al. (2022) investigated pitch-to-diameter ratio and aerofoil profile at high wind speeds of 8–10 m/s without systematically isolating blade angle as an independent variable under low wind speed conditions. Herraprastanti and Saputro (2021) simultaneously varied both blade angle and blade number, making it difficult to determine the independent contribution of blade angle alone. Ansari et al. (2021) conducted a CFD analysis at 5 m/s confirming that a 70° blade angle achieved the highest efficiency of 30.3%, yet evaluated only a single configuration, leaving the comparative performance across a broader angular range unaddressed. Ortiz-Velázquez et al. (2026) and Faisal et al. (2025) advanced ASWT optimization through multi-parameter and surface modification approaches respectively. While Syaukani et al. (2024) demonstrated blade optimization for Indonesian horizontal axis wind turbine (HAWT) conditions using blade element momentum (BEM) theory, none of these studies systematically isolated blade angle as a single variable under low wind speed conditions. Furthermore, the investigations were not conducted using CFD, which provides greater fidelity for capturing the complex flow phenomena inherent to helical blade structures. Mutasher (2024) employed CFD using ANSYS-CFX with the k-ω SST turbulence model to investigate small-scale ASWT performance. The study reported a maximum power coefficient of 0.2 at a TSR of 1.5. However, the investigation was limited to a fixed blade opening angle of 60°, leaving the effect of blade angle variation unexamined. Faroja et al. (2026) conducted a seven-day field experiment in Palembang-Indonesia comparing three and four-blade ASWT configurations under low wind speeds (0.8–4 m/s). The four-bladed turbine achieved superior performance, reaching 0.29 W at a wind speed of 4 m/s due to improved torque continuity and rotational stability. However, the study was limited to a fixed pitch angle of 60° and a short testing duration. Song et al. (2025) used CFD to analyze the effects of winglet geometry on ASWT performance. The study found that a 135° winglet angle with a length of 6–7% of the rotor diameter increased the peak Cp by 13.4% through tip vortex suppression.

Based on the foregoing review, the following research gaps are identified: first, most prior ASWT studies investigated blade angles only within a limited range of 50–70°, leaving the aerodynamic behavior at lower angles below 50° unexplored; second, many studies varied multiple geometric parameters simultaneously, making it impossible to isolate the independent effect of blade angle; third, the majority of studies employed wind speeds of 8 m/s or above, which are unrepresentative of Indonesian conditions, with the only exception being Ansari et al. (2021) whose analysis was restricted to a single blade angle; and fourth, CFD-based investigations systematically covering a wide angular range at low wind speeds remain scarce compared to BEM-based approaches, which are less suited to the complex spiral geometry of the ASWT.

Thus, there is a clear need to improve the understanding of how blade inclination angle alone influences the aerodynamic efficiency of an ASWT under realistic low-wind conditions,

particularly in relation to their application in sustainable and decentralized energy systems. Addressing this issue is important not only from an aerodynamic design perspective but also from an environmental engineering standpoint, as small scale wind technologies contribute to reducing dependence on fossil fuels and supporting low carbon energy transitions in regions with limited and unstable energy infrastructure.

In this context, the study is guided by the hypothesis that increasing the blade inclination angle enhances the aerodynamic interaction between the incoming airflow and the helical blade surface, resulting in improved momentum transfer, higher torque generation, and increased power output under low wind speed conditions. It is also hypothesized that higher inclination angles intensify wake formation due to greater energy extraction from the flow, leading to a more pronounced velocity deficit downstream of the turbine. Therefore, this study aims to evaluate the effect of blade inclination angle variations (30°, 35°, 40°, 45°, 50°, and 60°) on the aerodynamic performance and energy extraction capability of an ASWT operating at a low wind speed of 5 m/s using CFD. The objective is to identify configurations that maximize energy conversion efficiency while maintaining stable flow behavior, thereby enhancing the applicability of such turbines for sustainable decentralized renewable energy systems in low-wind environments.

NUMERICAL METHOD

Turbine geometry and computational domain

Figure 1 illustrates the three-dimensional geometry of the Archimedes wind turbine model, showing (a) the isometric view revealing the helical blade configuration and overall rotor geometry, and (b) the front view displaying the spiral blade arrangement and rotational symmetry of the three-bladed rotor assembly. The ASWT geometry was designed using SolidWorks 3D CAD 2022. The turbine consists of three helical blades arranged symmetrically around a central shaft. Six independent geometry models were created, each corresponding to one blade inclination angle: 30°, 35°, 40°, 45°, 50°, and 60°. All other geometric parameters were kept constant across all six models to ensure that blade angle is the sole independent variable. The principal geometric parameters are summarised in Table 1. Each model was exported in IGES format and imported into ANSYS Fluent 2021 R1 for pre-processing, meshing, and simulation.

The computational domain for the Archimedes wind turbine CFD simulation was designed as a rectangular box enclosure, as illustrated in Figure 2. The domain dimensions were carefully selected to ensure accurate flow field predictions while minimizing computational cost.The domain extends 7.5 m upstream of the rotor center to guarantee a fully developed, undisturbed inlet velocity profile, and 15 m downstream to adequately capture the near and far wake recovery regions without interference from the pressure outlet boundary condition. The lateral and vertical extents of the domain were each set to 15 m from the rotor axis, yielding a total cross-sectional area of 15 × 15 m, which maintains a frontal blockage ratio well below the recommended 3% threshold, thereby preventing artificial flow acceleration around the turbine due to domain confinement effects. The total axial length of the domain is therefore approximately 22.5 m, resulting in an overall domain size of 22.5 × 15 × 15 m. Figure 2 illustrates the computational domain employed in the CFD simulation of the ASWT.

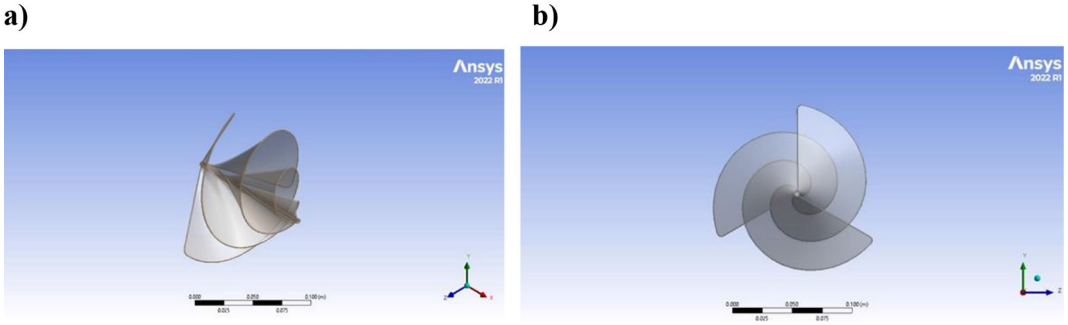

Figure 1. ASWT (a) isometric view, (b) front view

Table 1. Geometric parameters of the ASWT model

Parameter	Value	Unit
Rotor diameter	1.5	m
Turbine length	1.5	m
Blade thickness	0.01	m
Number of blades	3	–
Blade inclination angles	30, 35, 40, 45, 50, 60	degree (°)

Computational mesh

The computational mesh for the Archimedes wind turbine CFD simulation was generated using ANSYS Meshing, with the physics and solver preferences configured for ANSYS Fluent (see Figure 3). An unstructured tetrahedral mesh type was selected throughout the entire computational domain due to its ability to conform effectively to the complex helical blade geometry of the Archimedes wind turbine. The mesh was constructed using a two-zone strategy, where a coarser mesh was applied in the stationary outer domain and a significantly finer mesh was generated within the inner rotating zone surrounding the rotor assembly, as clearly visible from the mesh density contrast shown in the figures. The global maximum element size was set to 0.25 m for the outer domain, while the element size in the vicinity of the rotor and rotating zone was refined to between 0.20 mm and 0.25 mm. This local refinement ensures that the boundary layer flow, pressure gradients, and rotational wake structures induced by the helical blades are adequately resolved. A smooth transition between the refined and coarse mesh regions was achieved by controlling the growth rate, preventing abrupt changes in element size that could introduce numerical errors. Curvature-based mesh refinement was also applied to ensure that the curved surfaces of the helical blades were sufficiently captured by the mesh. The overall mesh quality was evaluated using the skewness and orthogonal quality criteria, and high smoothing was applied to improve element shape in regions of complex geometry. The resulting mesh achieved an average skewness value of 0.35 and an orthogonal quality of 0.65, both of which fall within the good range according to ANSYS Fluent mesh quality standards. The computational mesh of the ASWT is shown in Figure 3.

CFD simulation setup and boundary conditions

The CFD simulation of the ASWT was conducted using ANSYS Fluent 2021 R1 in three-dimensional, transient mode with a pressure-based solver and absolute velocity formulation. The working fluid was defined as air with a constant density of 1.225 kg/m³, a dynamic viscosity of 1.7894×10^{-5} kg/(m·s), and a specific heat capacity of 1006.43 J/(kg·K), representing standard atmospheric conditions at sea level. The turbulence was modelled using the standard k-epsilon (k-ε)

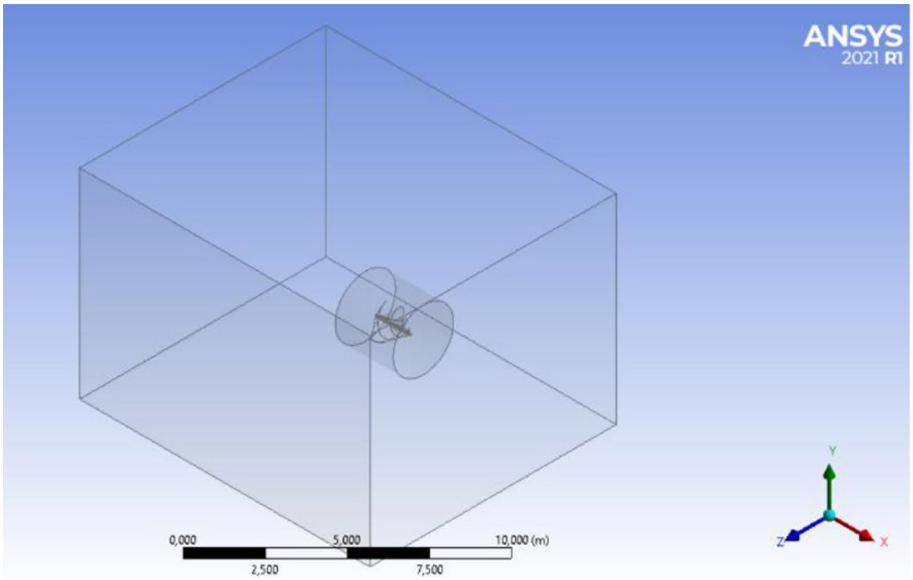

Figure 2. The computational domain of the ASWT

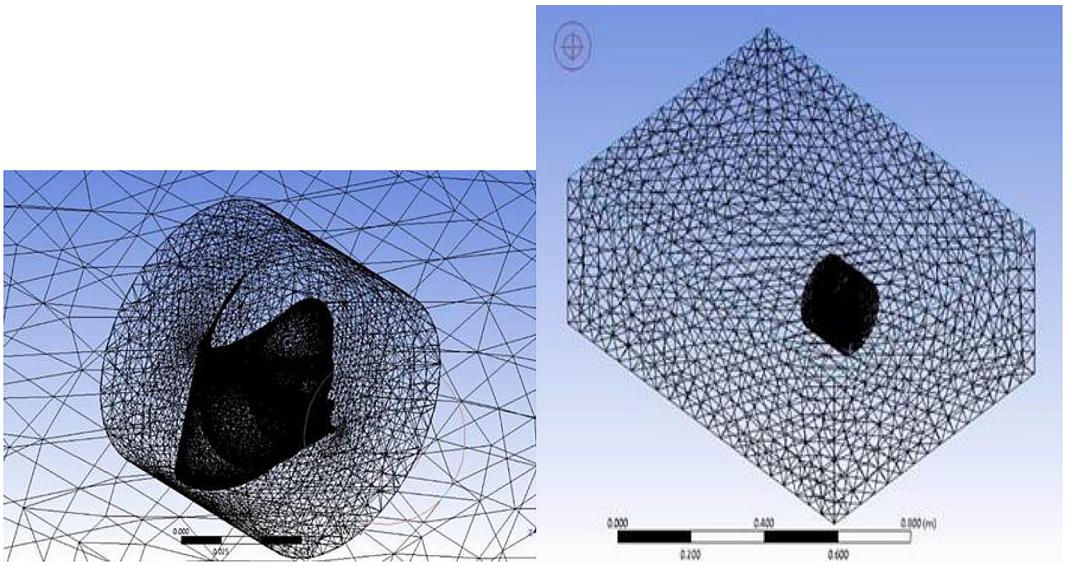

Figure 3. Computational mesh of the ASWT

turbulence model with standard wall functions applied to all solid wall boundaries, which is widely adopted in wind turbine CFD studies due to its robustness and computational efficiency in handling fully turbulent external flows.

Regarding the boundary conditions, the inlet face of the computational domain was assigned a uniform velocity inlet condition with a velocity magnitude of 5 m/s directed along the axial direction, representing the freestream wind speed. The outlet face was set as a pressure outlet with zero-gauge pressure, allowing the flow to exit the domain freely without inducing backflow effects. All remaining outer faces of the stationary domain, including the lateral and top and bottom walls, were treated as stationary no-slip walls. The turbine blade surfaces were similarly assigned a no-slip stationary wall boundary condition, ensuring that the viscous effects on the blade surfaces were properly captured. The interface between the stationary outer domain and the inner rotating zone was handled through a sliding mesh interface, defined as contact region source and target pairs, enabling the transfer of flow information across the two zones during the transient simulation.

For the cell zone conditions, the inner rotating zone was configured with mesh motion enabled at a rotational speed of 6.6 rad/s about the x-axis, corresponding to the operating rotational speed of the Archimedes wind turbine, while the stationary outer domain was assigned no frame motion and no mesh motion. The solution was initialized using the hybrid initialization method, which provides a more physically consistent initial flow field compared to standard initialization. The transient simulation was run with a time step size of 0.01 s, a total of 400-time steps, and a maximum of 50 iterations per time step, giving a total simulated physical time of 4 seconds, sufficient to capture the periodic behavior of the rotating turbine.

Governing equations

The continuity equation expresses the conservation of mass for a fluid flow and is given as follows (Anderson, 1995).

$$\frac{\partial \rho}{\partial t} + \nabla \cdot (\rho \vec{u}) = 0 \tag{1}$$

For the unsteady incompressible flow considered in this study, where the fluid density ρ is assumed constant, the continuity equation retains its time-dependent form and simplifies to:

$$\nabla \cdot \vec{u} = 0 \tag{2}$$

where: ρ is the fluid density (kg/m³), t is time (s), and $\vec{u}$ is the velocity vector (m/s).

The conservation of momentum for a viscous, incompressible fluid is described by the Navier-Stokes equations. For unsteady incompressible flow, the unsteady Reynolds-Averaged Navier-Stokes (URANS) equation is expressed as (Versteeg and Malalasekera, 2007):

$$\rho \frac{\partial \vec{u}}{\partial t} + \rho(\vec{u} \cdot \nabla)\vec{u} = -\nabla p + \mu \nabla^2 \vec{u} + \vec{F} \tag{3}$$

In component form for the x, y, and z directions:

$$\rho\left(\frac{\partial u}{\partial t}+u\frac{\partial u}{\partial x}+v\frac{\partial u}{\partial y}+w\frac{\partial u}{\partial z}\right)=$$

$$=-\frac{\partial p}{\partial x}+\mu\left(\frac{\partial^2 u}{\partial x^2}+\frac{\partial^2 u}{\partial y^2}+\frac{\partial^2 u}{\partial z^2}\right)+F_x \quad (4)$$

$$\rho\left(\frac{\partial v}{\partial t}+u\frac{\partial v}{\partial x}+v\frac{\partial v}{\partial y}+w\frac{\partial v}{\partial z}\right)=$$

$$=-\frac{\partial p}{\partial y}+\mu\left(\frac{\partial^2 v}{\partial x^2}+\frac{\partial^2 v}{\partial y^2}+\frac{\partial^2 v}{\partial z^2}\right)+F_y \quad (5)$$

$$\rho\left(\frac{\partial w}{\partial t}+u\frac{\partial w}{\partial x}+v\frac{\partial w}{\partial y}+w\frac{\partial w}{\partial z}\right)=$$

$$=-\frac{\partial p}{\partial z}+\mu\left(\frac{\partial^2 w}{\partial x^2}+\frac{\partial^2 w}{\partial y^2}+\frac{\partial^2 w}{\partial z^2}\right)+F_z \quad (6)$$

where: p is the static pressure (Pa), μ is the dynamic viscosity (Pa·s), and F_x, F_y, F_z are the body force components (N/m³) in each respective direction.

The additional time-derivative terms $\frac{\partial u}{\partial t}$, $\frac{\partial v}{\partial t}$, $\frac{\partial w}{\partial t}$, in each component equation represent the local rate of change of velocity with respect to time (m/s²). The conservation of energy for fluid flow is described by the energy equation, which accounts for heat transfer and viscous dissipation (Anderson, 1995):

$$\rho c_p\frac{DT}{Dt}=\nabla\cdot(k\nabla T)+\Phi \quad (7)$$

which can be written in expanded form as:

$$\rho c_p\left(\frac{\partial T}{\partial t}+\vec{u}\cdot\nabla T\right)=\nabla\cdot(k\nabla T)+\mu\Phi_v \quad (8)$$

where: T is the temperature (K), c_p is the specific heat capacity (J/kg·K), k is the thermal conductivity (W/m·K), and Φ_v is the viscous dissipation function.

Since the flow in this study is assumed to be isothermal and incompressible at low wind speeds, the energy equation is simplified and the thermal effects are considered negligible.

Turbulence model and wall functions

To model turbulence effects, the Standard k-epsilon (k-ε) turbulence model with standard wall functions was employed (Launder and Spalding, 1974). This well-established approach offers an appropriate balance between numerical accuracy and computational efficiency, making it particularly suitable for the present parametric study involving multiple blade inclination angles ranging from 30° to 60°. The governing transport equations for k and ε in their unsteady form are expressed as follows:

Turbulent kinetic energy (k):

$$\frac{\partial(\rho k)}{\partial t}+\frac{\partial(\rho k u_i)}{\partial x_i}=$$

$$=\frac{\partial}{\partial x_j}\left[\left(\mu+\frac{\mu_t}{\sigma_k}\right)\frac{\partial k}{\partial x_j}\right]+G_k-\rho\varepsilon \quad (9)$$

Turbulent dissipation rate (ε):

$$\frac{\partial(\rho\varepsilon)}{\partial t}+\frac{\partial(\rho\varepsilon u_i)}{\partial x_i}=$$

$$=\frac{\partial}{\partial x_j}\left[\left(\mu+\frac{\mu_t}{\sigma_\varepsilon}\right)\frac{\partial\varepsilon}{\partial x_j}\right]+C_{1\varepsilon}\frac{\varepsilon}{k}G_k-C_{2\varepsilon}\rho\frac{\varepsilon^2}{k} \quad (10)$$

where: the turbulent viscosity μ_t is computed as:

$$\mu_t=\rho C_\mu\frac{k^2}{\varepsilon} \quad (11)$$

where: ρ is the fluid density (kg/m³), u_i is the velocity component in the x_i direction (m/s), μ is the dynamic viscosity (Pa·s), μ_t is the turbulent viscosity (Pa·s), G_k represents the generation of turbulent kinetic energy due to mean velocity gradients (kg/m·s³), and σ_k and σ_ε are the turbulent Prandtl numbers for k and ε, respectively.

To handle the near-wall flow region without requiring an excessively fine mesh at the blade surfaces and domain walls, the standard wall functions approach was employed. The standard wall functions are valid within a dimensionless wall distance of $30 \le y^+ \le 300$, where y^+ is defined as:

$$y^+=\frac{\rho\mu_t y_p}{\mu} \quad (12)$$

where: ρ is the fluid density (kg/m³), u_τ is the friction velocity (m/s), y_p is the normal distance from the wall to the centroid of the first computational cell (m), and μ is the dynamic viscosity (Pa·s)

Performance parameter calculation

The turbine performance was evaluated based on two primary parameters: mechanical power

output and turbine efficiency. The mechanical power output was calculated from the torque generated by the rotating blade using the following equation (Burton et al., 2011):

$$P = T \cdot \omega \tag{13}$$

where: P is the mechanical power (W), T is the torque (N·m), and ω is the angular velocity (rad/s).

The turbine efficiency, expressed as the power coefficient (C_p), represents the fraction of wind power converted into mechanical power and is calculated as (Burton et al., 2011) :

$$C_p = \frac{P}{\frac{1}{2}\rho A V^3} \tag{14}$$

where: A is the swept area of the turbine rotor (m²) and V is the incoming wind speed (m/s).

The theoretical maximum value of C_p is 0.593, known as the Betz limit, which defines the upper boundary of energy extraction from wind by any wind turbine (Manwell et al., 2009; Bhatia, 2014).

The convergence criterion was determined by evaluating the level of agreement between the numerical simulation outcomes and the analytical reference results, in line with established CFD verification and validation procedures for wind turbine analysis. To ensure computational stability and accuracy, the CFD procedure involved a sequence of critical steps, namely geometry preparation, mesh generation, boundary condition assignment, and solver configuration. This research implemented a hybrid modeling workflow, using SolidWorks for initial geometry construction and ANSYS for detailed aerodynamic analysis. Within ANSYS, the modeling process included the incorporation of supporting geometry, specification of boundary conditions, mesh creation, and solver setup prior to the commencement of simulation (Wang et al., 2016; Sridhar et al., 2026).

RESULTS AND DISCUSSION

Validation results

The CFD simulation results of the ASWT were validated using the results reported by Ansari et al. (2021), with both turbines operating at a wind speed of 5 m/s (Figure 4). The validation results demonstrate a consistent agreement between the CFD predictions and the reference (validation) data across the investigated range of power coefficients (Cp). As shown in the figure, both datasets exhibit a similar increasing

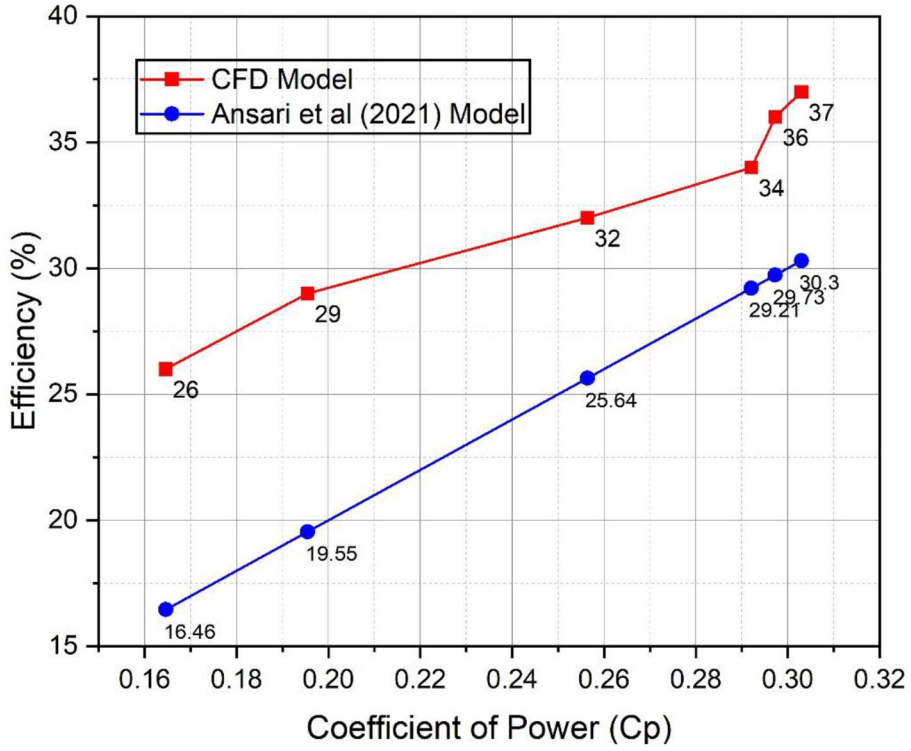

Figure 4. CFD validation results compared with previous studies on ASWT

trend in efficiency with rising Cp, indicating that the numerical model successfully captures the underlying physical behavior of the wind turbine. The CFD results slightly overpredict the efficiency compared to the validation data, with deviations ranging from approximately 10% at lower Cp (0.1646) to about 6–7% at higher Cp values (0.3030). As shown in the figure, the gap between the two curves decreases as Cp increases, indicating improved model accuracy at higher operating conditions. The overprediction observed in the Archimedes wind turbine simulation results can be attributed to differences in blade inclination angle, rotational speed, and the smaller model scale adopted by Ansari et al. (2021), all of which contribute to discrepancies in the predicted power output. These variations in power output, in turn, affect the calculated efficiency values. Overall, the good agreement in trends and the relatively small deviations confirm that the CFD model is sufficiently reliable for predicting turbine performance, and it can be considered valid for further parametric and design studies.

Torque simulation results

Figure 5 demonstrates that a larger blade inclination angle results in higher torque output from the wind turbine. Torque is a fundamental parameter in wind turbine performance, as it represents the rotational force that drives the shaft and enables energy conversion from wind kinetic energy into mechanical energy (Castillo et al., 2023). At an angle of 30°, the torque generated was 3.195 N.m, whereas at 60° it increased to 4.501 N.m. This trend indicates that torque rises with increasing inclination angle, despite constant wind speed and rotational speed applied to each ASWT. The blade inclination angle exerts a direct influence on torque generation in an ASWT by governing the momentum exchange between the incoming airflow and the helical blade surfaces. At lower inclination angles, the projected area normal to the flow is limited, resulting in weaker pressure differentials and a reduced tangential force component, thereby producing relatively low torque. As the inclination angle increases, the effective interaction between the flow and blade surface is enhanced, leading to stronger pressure gradients and a greater tangential force that contributes to torque. This improvement continues up to an optimal inclination angle, where the balance between lift- and drag-induced forces maximizes the torque output (Faisal et al., 2025). Since mechanical power is directly defined as the product of torque and angular velocity, expressed as in Equation 13, a higher torque value at a constant rotational speed will directly produce greater mechanical power output (Herlambang et al., 2023; Syaukani et al., 2024)

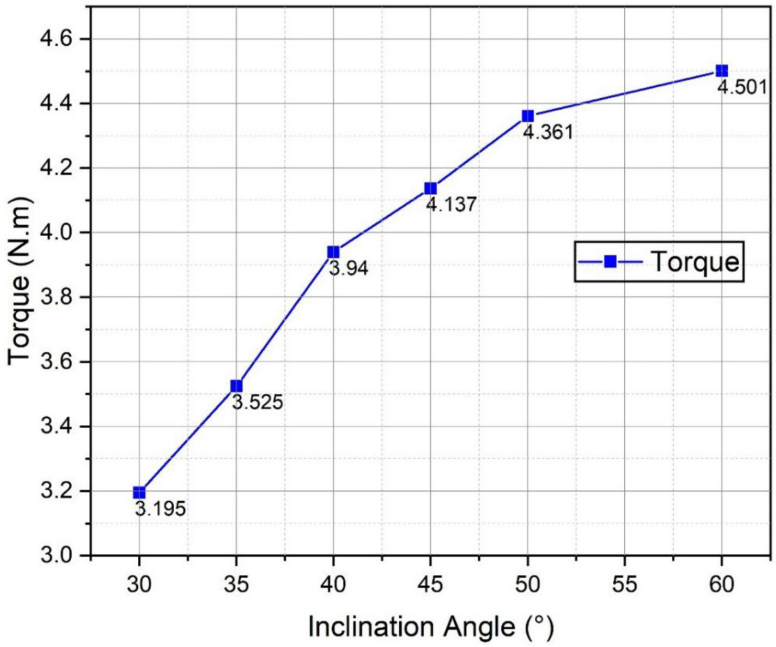

Figure 5. Relationship between torque and inclination angle

Turbine power analysis

Figure 6 shows the relationship between turbine power and blade inclination angle. As we can see from the figure that a steep rise in turbine power was observed as the inclination angle increased from 30° to 40°, attributable to the rapid improvement in the blade's effective wind-capturing area. When the blade inclination changes from 40° to 50°, the increase in turbine power proceeds at a more moderate rate. These findings suggest a significant turbine power rise as the inclination angle increases from 30° to 50°. This is primarily due to the corresponding increase in torque and improved aerodynamic interaction between the airflow and the helical blade surface. At lower angles, a larger portion of the aerodynamic force acts in the axial direction, limiting effective rotational work. However, increasing the inclination angle reorients the force components, enhancing tangential force and thereby increasing mechanical power output in line with the torque-angular velocity principles, while the helical blade geometry facilitates more continuous momentum transfer along the blade length at higher inclination angles, thereby enhancing overall energy extraction efficiency. Beyond 50°, the power curve transitioned into a near-plateau regime, with only a marginal gain of 0.92 W (~3,2%) observed up to 60°, reflecting the onset of aerodynamic saturation, where increasing the inclination angle yields progressively smaller improvements in power. The lowest power output was observed at 30°, with a value of 21.076 W, while the highest was obtained at 60°, reaching 29.691 W. The variation in power output across different angles is directly linked to the differences in torque generated, as expressed in Equation 13, where turbine power is the product of torque and rotational speed. These differences arise despite identical operating conditions for all ASWT, including constant wind speed, rotor diameter, and rotational speed. Power output reflects the turbine's capacity to convert wind kinetic energy into mechanical energy, where a higher power output under identical operating conditions inherently yields a higher power coefficient (Cp) and thus indicates superior aerodynamic performance (Firoozi et al., 2024). This result is consistent with the findings of Ansari et al. (2021) who conducted a CFD analysis of the ASWT at the same wind speed of 5 m/s and reported that the model with the largest blade opening angle of 70° produced the maximum power output and the highest Cp of 30.3%, directly confirming that larger blade angle configurations yield better turbine performance under identical low wind speed conditions.

Pressure contours of the wind turbine

The wind flow generates pressure on the turbine surface, as shown by the pressure contours in

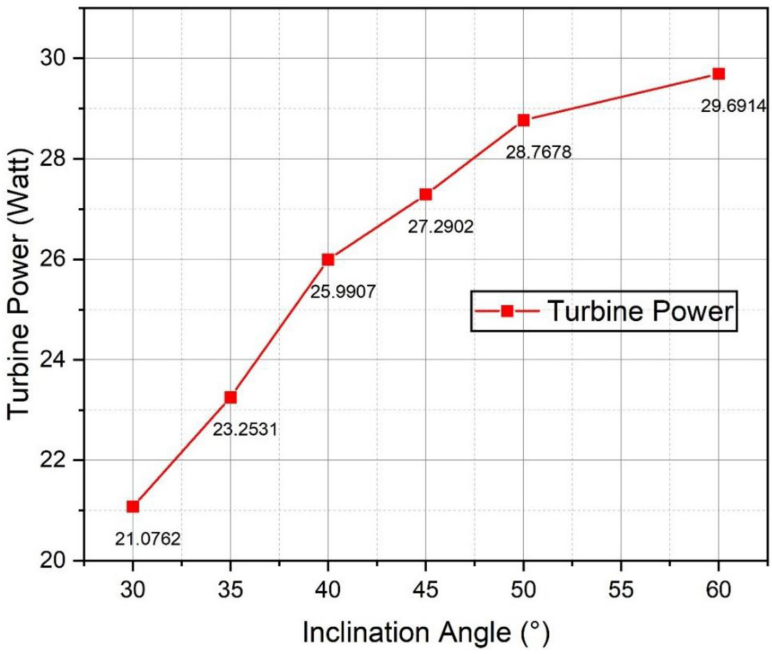

Figure 6. Relationship between turbine power and inclination angle

Figures 7 and 8. The red pressure region almost entirely covers the turbine surface, indicating that a larger blade angle generates greater pressure on the turbine. At a blade angle of 60°, the pressure distribution extends over a wider area of the blade surface, whereas at 30° the red region is concentrated mainly along the blade edges. Compared with the 30° configuration, the 60° turbine exhibits a broader high-pressure region extending from the blade center to its outer edges. These differences are primarily attributed to the variation in blade angle. In wind turbine aerodynamics, the pressure difference between the high- and low-pressure regions across the blade surface is the main mechanism generating the aerodynamic force responsible for rotation. A wider and more uniform pressure distribution is therefore associated with greater rotor force and higher power output (Ansari et al., 2021). Song et al. (2022) similarly reported that ASWT rotors with larger blade angles exhibited broader pressure distributions, a wider operating tip speed ratio range, and a higher power coefficient, confirming that surface pressure coverage is a key indicator of aerodynamic performance.

Velocity contour of the wind turbine

The velocity contour presented in Figure 9 illustrates the airflow behavior around the ASWT and reveals several key aerodynamic phenomena that govern its performance. Upstream of the turbine, the flow maintains a relatively uniform velocity distribution, indicating stable inlet conditions. As the air approaches the rotor region, a noticeable deceleration occurs, evidenced by the transition from higher velocity to lower velocity zones in front of and within the turbine enclosure. This reduction in velocity reflects the extraction of kinetic energy by the rotor blades. Within the rotor region, localized high-velocity gradients and small zones of accelerated flow are observed near the blade tips, suggesting the presence of strong shear layers and rotational effects induced by the helical blade geometry. Downstream of the turbine, a pronounced wake region is formed, characterized by reduced velocity and elongated flow structures extending along the streamwise direction. This wake indicates energy loss and flow separation, which are typical in wind energy conversion systems.

Figures 10 and 11 show the comparison wake region of the ASWT, spaced 2.5 m apart, between 30° and 60° blade angle, which shows notable differences. In Figure 10, both the near-wake and far-wake contours at the center are dominated by a yellow-green color, indicating that the turbine's outgoing airflow has relatively low velocities, ranging from 2 to 3.5 m/s. In contrast, in Figure 11, the central regions of the near-wake and far-wake contours are dominated by yellow-red colors, signifying higher outgoing airflow velocities of 3.8 to 4.6 m/s, which indicates that the wind speed leaving the turbine is only slightly reduced

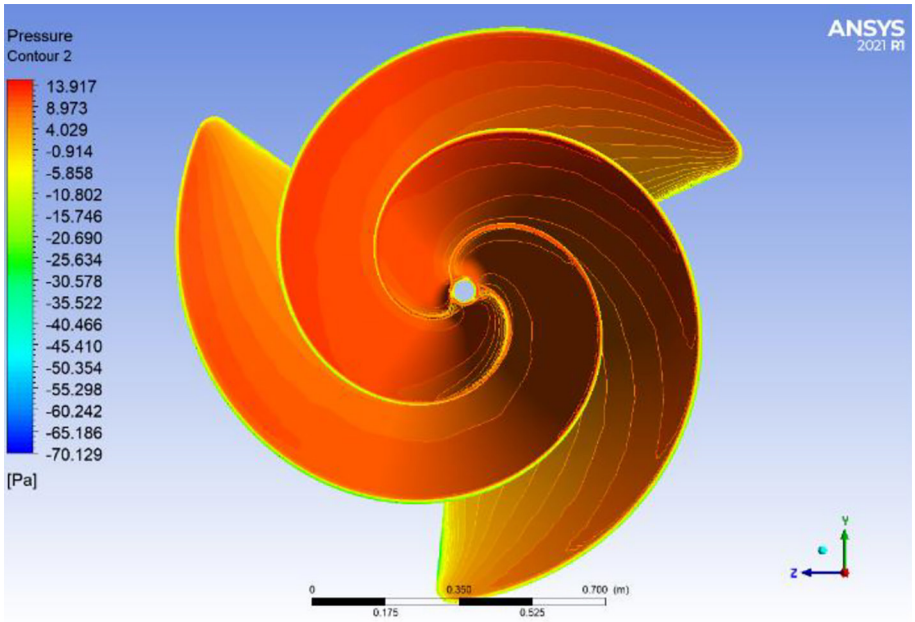

Figure 7. Pressure contour of the wind turbine at a 60° blade angle

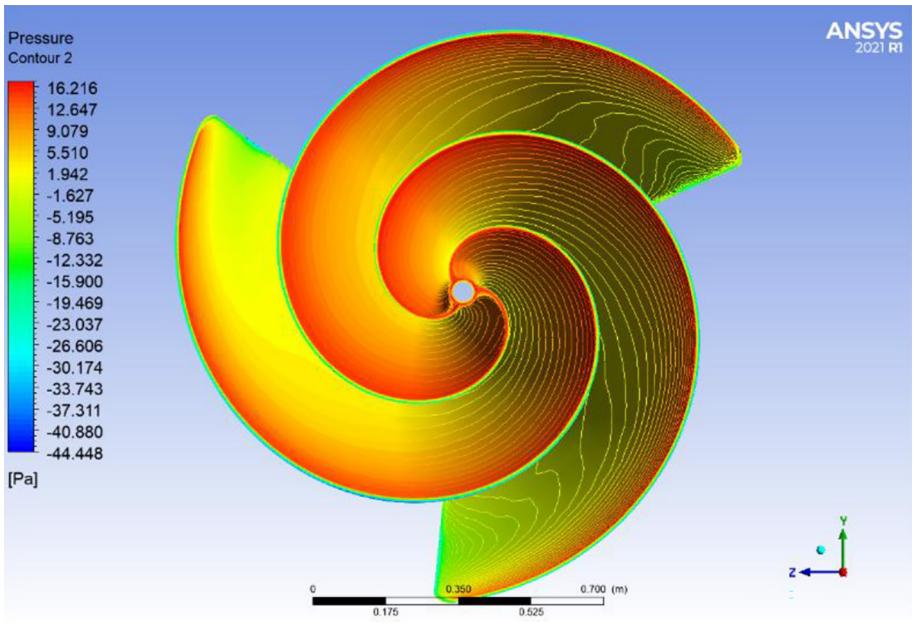

Figure 8. Pressure contour of the wind turbine at a 30° blade angle

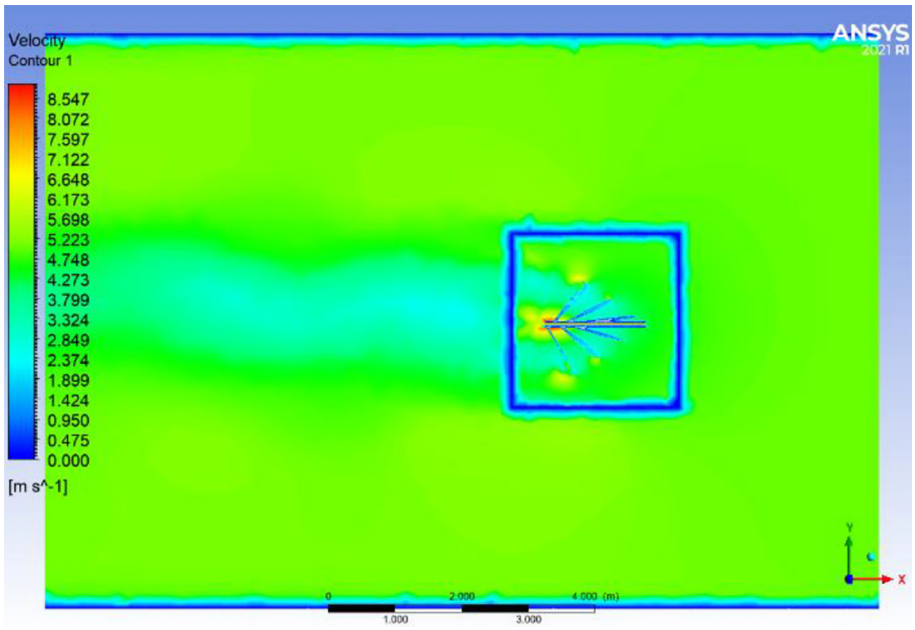

Figure 9. Air velocity contour around the wind turbine

compared to the incoming wind speed of 5 m/s. From an aerodynamic standpoint, a greater reduction in wake velocity relative to the freestream wind speed signifies that more kinetic energy has been absorbed by the rotor and converted into mechanical work, corresponding to higher turbine efficiency and power output (Firoozi et al., 2024). In this regard, Song et al. (2022) demonstrated through numerical simulation on ASWT rotors with different blade angles that rotors with larger blade angles produced a more structured wake pattern with greater momentum exchange between the rotor and the incoming airflow, which was directly associated with a wider operating tip speed ratio range and a higher maximum power coefficient. Therefore, the lower and more uniform wake velocity observed in the 60° configuration indicates more effective and spatially consistent energy extraction across the blade surface, confirming that this configuration achieves superior aerodynamic performance compared to the 30° configuration.

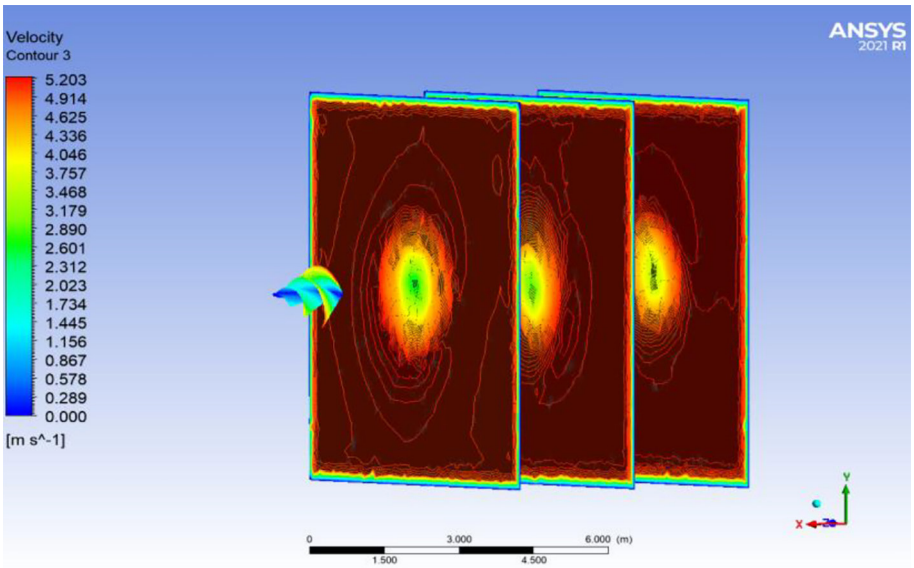

Figure 10. Wake-affected area of the turbine at a 60° blade angle

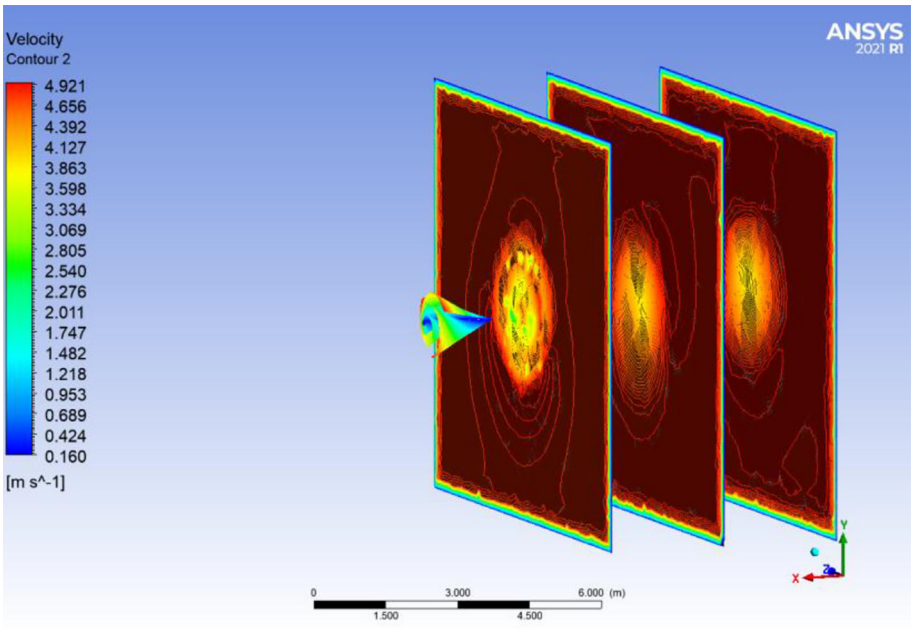

Figure 11. Wake region of the turbine with a 30° blade angle

In addition to velocity contours, the airflow around the turbine blades is depicted in Figure 12. A side view corresponding to Figure 12 is illustrated in Figure 13 for clarity. As we can see form the figures that the airflow changes after passing over the turbine blades, particularly in terms of velocity. At the central region of the turbine, the wind speed increases from the initial 5 m/s to 6.906 m/s after passing the blades. In contrast, airflow along the inner and outer edges of the blades decreases from the initial 5 m/s to a range of 2.302–4.604 m/s. Figure 13 also shows that the airflow becomes slightly turbulent after passing over the turbine blades.

CONCLUSIONS

The CFD analysis demonstrated that blade inclination angle governs both the energy extraction capability and wake development of the ASWT under low-wind-speed operating conditions. Increasing the blade inclination angle from 30° to 60° systematically enhanced aerodynamic

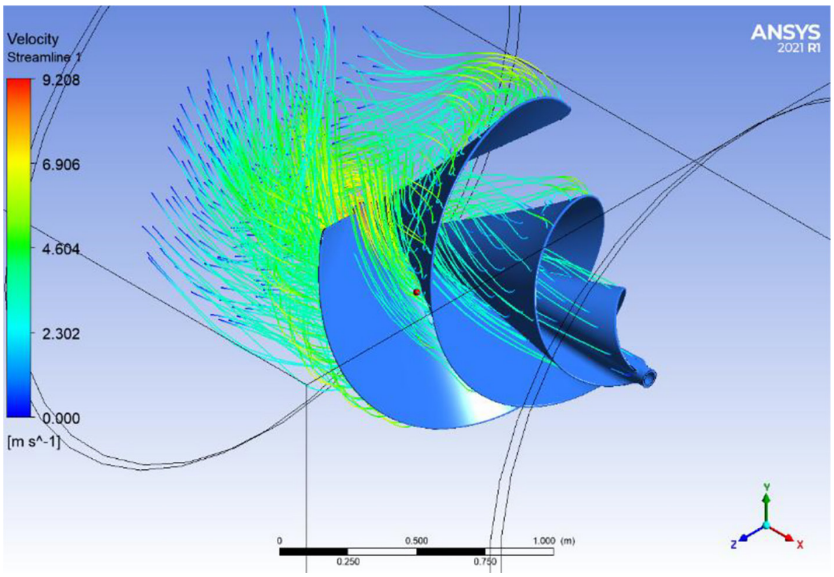

Figure 12. Downstream flow of the wind turbine

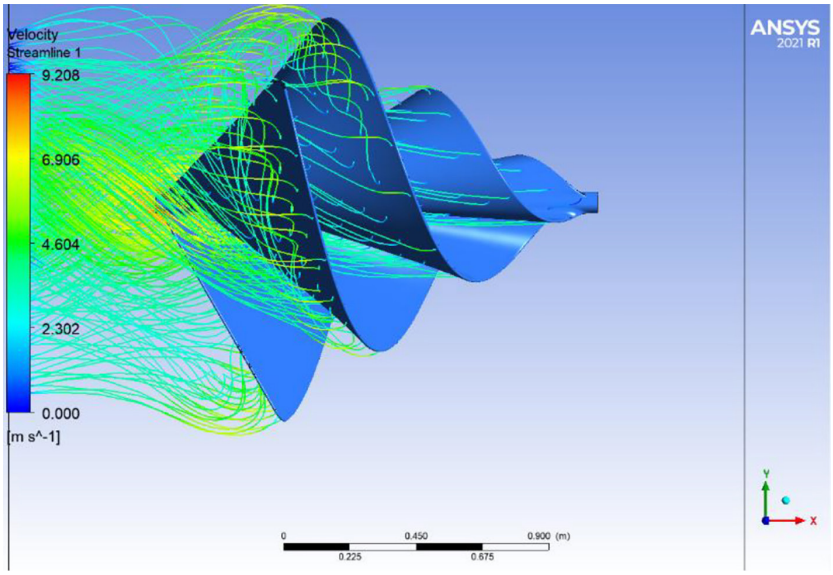

Figure 13. Airflow over the wind turbine blade

performance by increasing the interaction between the incoming airflow and the helical blade surface, resulting in greater tangential force generation and improved momentum transfer.

Among the investigated configurations, the 60° blade angle achieved the highest aerodynamic performance, producing a torque of 4.501 N.m, a mechanical power output of 29.691 W, and a power coefficient of 37%, whereas the 30° configuration exhibited the lowest performance, with 3.195 N·m torque, 21.076 W power output, and 26% efficiency. The increase in turbine performance with blade angle was associated with broader pressure distribution over the blade surface, stronger wake velocity deficit, and more effective kinetic energy extraction from the airflow. The wake analysis revealed that larger blade inclination angles generate a more extended low-velocity wake region and slower downstream velocity recovery, indicating intensified aerodynamic loading and increased energy absorption by the rotor. In contrast, smaller blade angles produced weaker wake structures and lower momentum extraction, corresponding to reduced turbine efficiency. These findings establish a direct aerodynamic relationship between blade inclination angle, wake development, and renewable energy conversion performance in ASWT.

The study provides new numerical evidence that blade-angle modification can substantially improve low-speed wind energy harvesting in compact helical turbines without altering rotor diameter or operating wind conditions. The obtained results support the application of high-inclination ASWT configurations for decentralized small-scale renewable energy systems operating in low-wind environments, where stable energy extraction and compact turbine geometry are required.

REFERENCES

1. Anderson, J.D. (1995). *Computational fluid dynamics: The basics with applications*. McGraw-Hill.
2. Ardoin, N. M., Bowers, A. W. (2025). Collective action impacts on climate change mitigation. *Current Opinion in Behavioral Sciences*, *63*, 101503. https://doi.org/10.1016/j.cobeha.2025.101503
3. Ansari, A. S., Hussain, T., Hussain, A., Ali, I. (2021). Efficiency analysis of Archimedes wind turbine using CFD technique. *International Journal of Scientific & Engineering Research*, *12*(3). http://www.ijser.org
4. Bhatia, S.C. (2014). Wind energy. In *Advanced Renewable Energy Systems* (pp. 184–222). Elsevier. https://doi.org/10.1016/B978-1-78242-269-3.50008-5
5. Budiarto, A. W., Surjosatyo, A. (2021). Indonesia's Road to Fulfill National Renewable Energy Plan Target in 2025 and 2050: Current Progress, Challenges, and Management Recommendations – A Small Review. *IOP Conference Series: Earth and Environmental Science*, *940*(1), 012032. https://doi.org/10.1088/1755-1315/940/1/012032
6. Budiman, Y., Khoirunnisa', A. (2025). Predictive analysis of biofuel production in prominent Asian markets: Implications for renewable energy development (2045–2050). *IOP Conference Series: Earth and Environmental Science*, *1518*(1), 012009. https://doi.org/10.1088/1755-1315/1518/1/012009
7. Burton, T., Jenkins, N., Sharpe, D., Bossanyi, E. (2011). *Wind Energy Handbook*. Wiley. https://doi.org/10.1002/9781119992714
8. Castillo, O. C., Andrade, V. R., Rivas, J. J. R., González, R. O. (2023). Comparison of power coefficients in wind turbines considering the tip speed ratio and blade pitch angle. *Energies*, *16*(6), 2774. https://doi.org/10.3390/en16062774
9. Faisal, A. E., Lim, C. W., Al-Quraishi, B. A. J., Milano, J., Hong, T. C., Chen, C. P. (2025). Aerodynamic performance enhancement of Archimedes spiral wind turbine blades through surface modifications: A numerical and experimental study. *Scientific Reports*, *15*(1), 41112. https://doi.org/10.1038/s41598-025-24908-6
10. Faroja, A., Arifin, F., RS, C. (2026). Comparative of field study of three- and four-bladed archimedes spiral wind turbines under natural low wind conditions. *Jurnal Polimesin*, *24*(2), 200–206. https://e-jurnal.pnl.ac.id/polimesin/article/view/8908/5890
11. Firoozi, A. A., Hejazi, F., Firoozi, A. A. (2024). Advancing wind energy efficiency: A systematic review of aerodynamic optimization in wind turbine blade design. *Energies*, *17*(12), 2919. https://doi.org/10.3390/en17122919
12. Herlambang, Y. D., Prasetiyo, B., Alfauzi, A. S., Purwanto, W., Arifin, F., Emzain, Z. F. (2023). Optimization of savonius turbine towards different inner blade positions to improve turbine performance. *21*(1), 112–116. https://doi.org/http://dx.doi.org/10.30811/jpl.v21i1.3248
13. Herraprastanti, E. H., Saputro, W. A. (2021). Simulation of opening angle of Archimedes wind turbine design based on the Fibonacci series. *International Journal of Engineering, Science and Information Technology*, *2*(1), 50–57. https://doi.org/10.52088/ijesty.v2i1.192
14. Kamal, A. M., Nawar, M. A. A., Attai, Y. A., Mohamed, M. H. (2022). Blade design effect on Archimedes Spiral Wind Turbine performance: Experimental and numerical evaluations. *Energy*, *250*, 123892. https://doi.org/10.1016/j.energy.2022.123892
15. Kim, K., Ji, H., Kim, Y., Lu, Q., Baek, J., Mieremet, R. (2014). Experimental and numerical study of the aerodynamic characteristics of an Archimedes spiral wind turbine blade. *Energies*, *7*(12), 7893–7914. https://doi.org/10.3390/en7127893
16. Kusuma, Y. F., Fuadi, A. P., Hakim, B. Al, Sasmito, C., Nugroho, A. C. P. T., Khoirudin, M. H., Priatno, D. H., Tjolleng, A., Wiranto, I. B., Al Fikri, I. R., Muttaqie, T., Prabowo, A. R. (2024). Navigating challenges on the path to net zero emissions: A comprehensive review of wind turbine technology for implementation in Indonesia. *Results in Engineering*, *22*, 102008. https://doi.org/10.1016/j.rineng.2024.102008
17. Labib, A., AbdelGawad, A., Nasseif, M. (2020). Effect of aspect ratio on aerodynamic performance of archimedes spiral wind turbine. *The Egyptian International Journal of Engineering Sciences and Technology*, *32*(Mechanical Engineering), 66–72. https://doi.org/10.21608/eijest.2020.45256.1017
18. Launder, B. E., Spalding, D. B. (1974). The numerical computation of turbulent flows. *Computer Methods in Applied Mechanics and Engineering*, *3*, 269–289. https://doi.org/10.1016/0045-7825(74)90029-2
19. Manwell, J. F., McGowan, J. G., Rogers, A. L. (2009). *Wind Energy Explained*. Wiley. https://doi.org/10.1002/9781119994367
20. Maulana, M. I., Syuhada, A., Hasan, A. (2024). Experimental investigation of the horizontal axis wind turbine with NACA4418 blade length. *Journal of Ecological Engineering*, *25*(9), 272–281. https://

doi.org/10.12911/22998993/191437

21. Mutasher, S. A. (2024). Performance investigation of Archimedes wind turbine using computational fluid dynamics (CFD) analysis. *2024 1st International Conference on Innovative Engineering Sciences and Technological Research (ICIESTR)*. https://doi.org/10.1109/ICIESTR60916.2024.10798314
22. Ortiz-Velázquez, D., Rosado-Tamariz, E., Campos-Amezcua, R., Blanco-Ortega, A., Claudio-Pachecano, L., Campos-Amezcua, A. (2026). Effect of aspect ratio on the performance of an enhanced Archimedes spiral wind turbine in urban conditions. *Results in Engineering*, *29*, 109056. https://doi.org/10.1016/j.rineng.2026.109056
23. Pambudi, N. A., Ulfa, D. K., Nanda, I. R., Gandidi, I. M., Wiyono, A., Biddinika, M. K., Rudiyanto, B., Saw, L. H. (2025). The Future of Wind Power Plants in Indonesia: Potential, Challenges, and Policies. *Sustainability*, *17*(3), 1312. https://doi.org/10.3390/su17031312
24. Pandyaswargo, A. H., Wibowo, A. D., Sunarti, S., Risnawati, Onoda, H. (2024). A needs-based approach to sustainable energy use: case studies of four remote villages in Indonesia. *Environment, Development and Sustainability*. https://doi.org/10.1007/s10668-024-05572-8
25. Song, K., Huan, H., Kang, Y. (2022). Aerodynamic performance and wake characteristics analysis of Archimedes spiral wind turbine rotors with different blade angle. *Energies*, *16*(1), 385. https://doi.org/10.3390/en16010385
26. Song, K., Huan, H. T., Wei, L. C., Liu, C. X. (2025). Performance analysis of a modified Archimedes spiral wind turbine having winglet on blade. *Energy*, *333*, 137389. https://doi.org/10.1016/j.energy.2025.137389
27. Sridhar. S, Raghavendra N K, Mohan Das R. (2026). Integrated theoretical and CFD study on the aerodynamic behaviour of a horizontal axis wind turbine. In *Tuijin Jishu/Journal of Propulsion Technology 47*(2). https://www.propulsiontechjournal.com/index.php/journal/article/view/10609/6266
28. Syaukani, M., Wahyu Aryadi, A., Dwi Arirohman, I., Edhy Sofyan, S., Harjon Bahar, A. (2024). Twist and chord optimization using the linearization method on the taper blade of a micro-horizontal axis wind turbine. *Jurnal Polimesin*, *22*(5), 2024–2031. http://e-jurnal.pnl.ac.id/polimesin
29. Versteeg, H.K., Malalasekera, W. (2007). *An Introduction to Computational Fluid Dynamics: The Finite Volume Method* (2nd ed.). Pearson Education Limited.
30. Wang, L., Quant, R., Kolios, A. (2016). Fluid structure interaction modelling of horizontal-axis wind turbine blades based on CFD and FEA. *Journal of Wind Engineering and Industrial Aerodynamics*, *158*, 11–25. https://doi.org/10.1016/j.jweia.2016.09.006